Supplement of Atmos. Meas. Tech., 9, 4547–4560, 2016
http://www.atmos-meas-tech.net/9/4547/2016/
doi:10.5194/amt-9-4547-2016-supplement

Atmospheric Measurement Techniques
Open Access
EGU

Supplement of

Inter-comparison of NIOSH and IMPROVE protocols for OC and EC determination: implications for inter-protocol data conversion

Cheng Wu et al.

Correspondence to: Jian Zhen Yu (jian.yu@ust.hk)

This document contains four supporting tables, twenty-four supporting figures, and description of one additional reconstruction approach other than the three described in the main text.

Descriptions of M3 reconstruction approach

Another reconstruction approach (M3) also utilizes the relationship of PC. Combining Equations 3 and 4 yields

$$EC_{IMP\_TOR} = EC_{NSH\_TOT} + OC4_{NSH} + \left(PC_{NSH\_TOT} - PC_{IMP\_TOR}\right) \quad \text{(S1)}$$

In Equation S1, PC_{IMP_TOR} is the only unknown term on the right hand side, and empirical regression is used to replace it with known variables leading to the third method (M3) for EC reconstruction

$$\boldsymbol{M3}: \quad EC_{IMP\_TOR} = EC_{NSH\_TOT} + OC4_{NSH} + a \times \left(PC_{NSH\_TOT} - PC_{NSH\_TOR}\right) + b \quad \text{(S2)}$$

Based on the linear relationship (Figure S11) between (PC_{NSH_TOT}-PC_{NSH_TOR}) and (PC_{NSH_TOT}-PC_{IMP_TOR}), EC_{IMP_TOR} can be estimated as shown in Equation S2.

Results of M2-1 and M3 reconstruction approaches

Reconstruction results on EC by M2-1 are shown in Figure S12a~b. The performance is similar between the two scenarios, and the R^2 by M2-1 is the highest among all four reconstruction approaches, which proves that including K^+ and Fe can improve the reconstruction comparing to M2. EC frequency distributions of M2-1 are shown in Figure S15 and Figure S16, which are similar to M2. OC reconstruction by M2-1 is shown in Figure S13, all of which exhibit close to unity slopes (0.95~0.96). The OC distributions (Figure S17 and S18) by M2-1 are sharper than those for M2, confirming the advantage of using MLR. The reconstructed OC/EC ratios by M2-1 are slightly underestimated from 15% to 18% as shown in Figure S14a~b. The bias is associated with the sharper OC/EC distribution by reconstruction compared to the measurements (Figure S19e~f)

The EC reconstruction results of M3 are shown in Figure S12c~d. M3 reconstruction by season (Figure S12c) and by site (Figure S12d) yield similar R^2. EC frequency distributions (Figures S15 and S16) also confirm that M3 can provide higher precision (narrower distributions) than M1, but with a higher bias (asymmetric distributions). OC reconstruction by M3 is slightly underestimated as shown in Figure S13c~d (slope 0.95~0.98). The OC distributions (Figures S17g~h and S18g~h) indicate that season and site parameter scenarios yield similar reconstruction results. The reconstructed OC/EC ratios by M3 are underestimated from 31% to 58% as shown in Figure S14c~d. The bias is due to a sharper OC/EC distribution by reconstruction compared to the measurements (Figures S19g~h and S20g~h).

SOC estimation by M2-1 and M3

The usability of reconstructed EC_{IMP_TOR} and OC_{IMP_TOR} for SOC estimation using M2-1 and M3 are investigated. To account for the temporal variations of $(OC/EC)_{pri}$, seasonal $(OC/EC)_{pri}$ are calculated using OC and EC reconstructed by M2-1 and M3 (Table S3). These $(OC/EC)_{pri}$ values are then subject to SOC estimation following Equation 13. It is very clear that the frequency distribution of reconstructed SOCs deviates from the native SOC (Figure S24a and S24c). SOCs by and M2-1 and M3 are both

underestimated by 32~34% by the regression slope. The moderate R^2 (Figure S24b and S24d) also suggests the SOC by reconstructed EC_{IMP_TOR} and OC_{IMP_TOR} are poorly correlated with SOC by measured EC_{IMP_TOR} and OC_{IMP_TOR}. Similar to the results shown in the main text, the significant bias and moderate correlations suggest that reconstructed EC_{IMP_TOR} and OC_{IMP_TOR} are not suitable for SOC estimation.

References

Chow, J. C., Watson, J. G., Chen, L. W. A., Chang, M. C. O., Robinson, N. F., Trimble, D., and Kohl, S.: The IMPROVE-A temperature protocol for thermal/optical carbon analysis: maintaining consistency with a long-term database, J. Air. Waste. Manage., 57, 1014-1023, doi:10.3155/1047-3289.57.9.1014, 2007.
Lin, P., Engling, G., and Yu, J. Z.: Humic-like substances in fresh emissions of rice straw burning and in ambient aerosols in the Pearl River Delta Region, China, Atmos. Chem. Phys., 10, 6487-6500, doi:10.5194/acp-10-6487-2010, 2010.
Tang, B., Chiang, Y., Baldwin, A., and Yeung, C.: Study of the integrated rail-property development model in Hong Kong, Research Centre for Construction & Real Estate Economics, Department of Building & Real Estate, Faculty of Construction & Land Use, the Hong Kong Polytechnic University, 2004.

Table S1. **Temperature ramping steps of the IMPROVE and NIOSH protocol.**

Carrier Gas	Carbon Fraction		NIOSH		IMPROVE [2]	
			T (°C) [1]	RT (s) [1]	T (°C)	RT (s)
Helium	AOC	OC1	310	80	120	150-580
		OC2	475	60	250	150-580
		OC3	615	60	450	150-580
		OC4	870	90	550	150-580
2% Oxygen in helium	AEC	EC1	550	45	550	150-580
		EC2	625	45	700	150-580
		EC3	700	45	800	150-580
		EC4	775	45		
		EC5	850	45		
		EC6	870	45		

[1] T: temperature (°C) and RT: Residence time (seconds).
[2] The IMPROVE temperature program was used for measurements reported in this work. Another related temperature protocol, termed IMPROVE_A, is typically adopted on DRI Model 2001 carbon analyzers. The IMPROVE_A temperature protocol defines temperature plateaus of 140 °C for OC1, 280 °C for OC2, 480 °C for OC3, and 580 °C for OC4 in a helium (He) carrier gas and 580 °C for EC1, 740 °C for EC2, and 840 °C for EC3 in a 98% He/2% oxygen (O_2) carrier gas (Chow et al., 2007). These temperatures used with the new hardware in DRI Model 2001 better match the sample temperatures experienced in the analysis using IMPROVE protocol on the previous models of OGC (Oregon Graduate Center) analyzers.

Table S2. $OC4_{NSH}/TC_{NSH}$ dependency on K^+/EC_{NSH} by independent t-test using SPSS.

Group Statistics

		N	Mean	Std. Deviation	Std. Error Mean
$OC4_{NSH}/TC_{NSH}$	low K^+	119	0.1407	0.05983	0.00548
	high K^+	122	0.2686	0.11182	0.01012

$OC4_{NSH}/TC_{NSH}$	Levene's Test for Equality of Variances		t-test for Equality of Means						
	F	Sig.	t	df	Sig. (2-tailed)	Mean Difference	Std. Error Difference	95% Confidence Interval of the Difference	
								Lower	Upper
Equal variances assumed	31.32	0.000	-11.03	239	0.000	-0.12786	.01159	-0.15	-0.105
Equal variances not assumed			-11.11	186	0.000	-0.12786	.01151	-0.15	-0.105

Table S3. $(OC/EC)_{pri}$ calculation using MRS for individual seasons.

Season	$(OC/EC)_{pri}$ calculated from measured OC and EC		$(OC/EC)_{pri}$ calculated from reconstructed OC and EC			
			IMPROVE TOR			
	NIOSH TOT	IMPROVE TOR	M1	M2	M2-1	M3
Spring	1.31	0.58	0.47	0.84	0.64	0.70
Summer	1.15	0.55	0.47	0.68	0.62	0.62
Fall	1.26	0.71	0.46	0.62	0.80	0.59
Winter	1.85	0.93	0.81	1.18	0.95	0.94

Table S4. Parameters for OC and EC reconstruction in Hong Kong.

Approach*				2011-2013		2011-2012		2011		2012		2013	
				a1,a2,a3	b	a1,a2,a3	b	a1,a2,a3	b	a1,a2,a3	b	a1,a2,a3	b
M2-1	by season		Spring	0.44		0.38		0.82		0.00		0.53	
				3.61	0.00	3.73	0.00	2.60	0.10	2.71	0.00	2.98	0.10
				0.00		0.00		0.42		0.42		0.00	
			Summer	0.02		0.00		0.23		0.00		0.06	
				2.68	0.02	2.74	0.00	2.49	0.00	3.32	0.00	1.94	0.00
				2.23		2.30		1.99		1.00		2.58	
			Fall	0.13		0.35		0.09		0.81		0.20	
				2.40	0.02	2.02	0.00	2.64	0.00	2.08	0.10	3.94	0.10
				2.42		2.07		0.00		0.87		0.00	
			Winter	1.04		0.96		1.01		0.72		1.15	
				1.29	0.10	1.22	0.10	1.13	0.10	2.51	0.00	1.37	0.10
				1.37		2.00		1.88		1.47		0.70	
	by site	Roadside	MK	0.57		0.47		0.63		0.17		0.71	
				2.46	0.00	2.64	0.00	2.02	0.00	3.12	0.00	2.25	0.00
				0.27		0.52		1.35		0.49		0.00	
		Urban	TW	1.04		1.22		1.29		1.00		0.73	
				1.63	0.00	1.33	0.00	1.06	0.00	1.70	0.00	2.02	0.00
				1.19		0.74		1.31		0.69		2.48	
			YL	0.76		0.81		0.48		1.07		0.66	
				1.89	0.00	1.75	0.06	1.64	0.01	2.09	0.00	2.09	0.00
				1.33		0.96		3.14		0.00		2.02	
			CW	0.98		0.95		0.86		1.13		0.99	
				1.18	0.00	1.09	0.00	0.61	0.00	2.25	0.00	1.38	0.00
				2.45		2.61		4.11		0.00		2.32	
			TC	0.95		0.93		0.87		1.03		0.94	
				1.63	0.00	1.54	0.06	1.38	0.10	2.29	0.00	1.75	0.00
				1.37		1.13		1.48		0.32		1.90	
			Urban sites combined	0.94		0.98		0.88		1.02		0.85	
				1.60	0.00	1.49	0.02	1.25	0.50	2.18	0.00	1.79	0.00
				1.47		1.19		2.10		0.26		2.12	
		Suburban	WB	1.42		1.60		1.51		1.44		1.14	
				1.13	0.10	0.90	0.10	0.60	0.10	1.98	0.00	1.21	0.10
				1.27		0.87		2.12		0.25		2.91	
				a	b	a	b	a	b	a	b	a	b
M3	by season		Spring	0.91	-0.17	1.02	-0.18	0.78	-0.12	1.04	-0.23	0.92	-0.23
			Summer	0.77	0.00	0.47	0.00	0.73	0.00	0.57	-0.11	1.30	-0.07
			Fall	0.71	-0.25	0.60	-0.19	0.92	-0.18	0.47	-0.39	0.97	-1.21
			Winter	0.60	-0.22	0.77	-0.37	1.67	-2.38	0.76	-0.24	0.49	-0.14
	by site	Roadside	MK	1.02	0.09	0.97	0.08	0.90	0.07	1.13	0.10	1.11	0.14
		Urban	TW	0.55	-0.01	0.48	0.00	0.55	0.01	0.40	0.00	0.85	-0.06
			YL	0.62	-0.01	0.56	-0.01	0.63	0.00	0.77	-0.23	0.75	-0.02
			CW	0.49	0.01	0.42	0.01	0.46	0.01	0.42	-0.10	0.69	-0.02
			TC	0.50	0.00	0.44	0.00	0.47	0.00	0.79	-0.19	0.81	-0.06
			Urban sites combined	0.54	0.00	0.48	0.00	0.53	0.00	0.56	-0.12	0.76	-0.04
		Suburban	WB	0.33	-0.09	0.23	-0.07	0.16	-0.06	0.63	-0.21	0.48	-0.13

*Reconstruction equations:

$$\boldsymbol{M2-1}: \quad EC_{IMP\_TOR} = AEC_{NSH} + OC4_{NSH} - (a_1 \times PC_{NSH\_TOR} + a_2 \times K^+ + a_3 \times Fe + b)$$

$$\boldsymbol{M3}: \quad EC_{IMP\_TOR} = EC_{NSH\_TOT} + OC4_{NSH} + a \times (PC_{NSH\_TOT} - PC_{NSH\_TOR}) + b$$

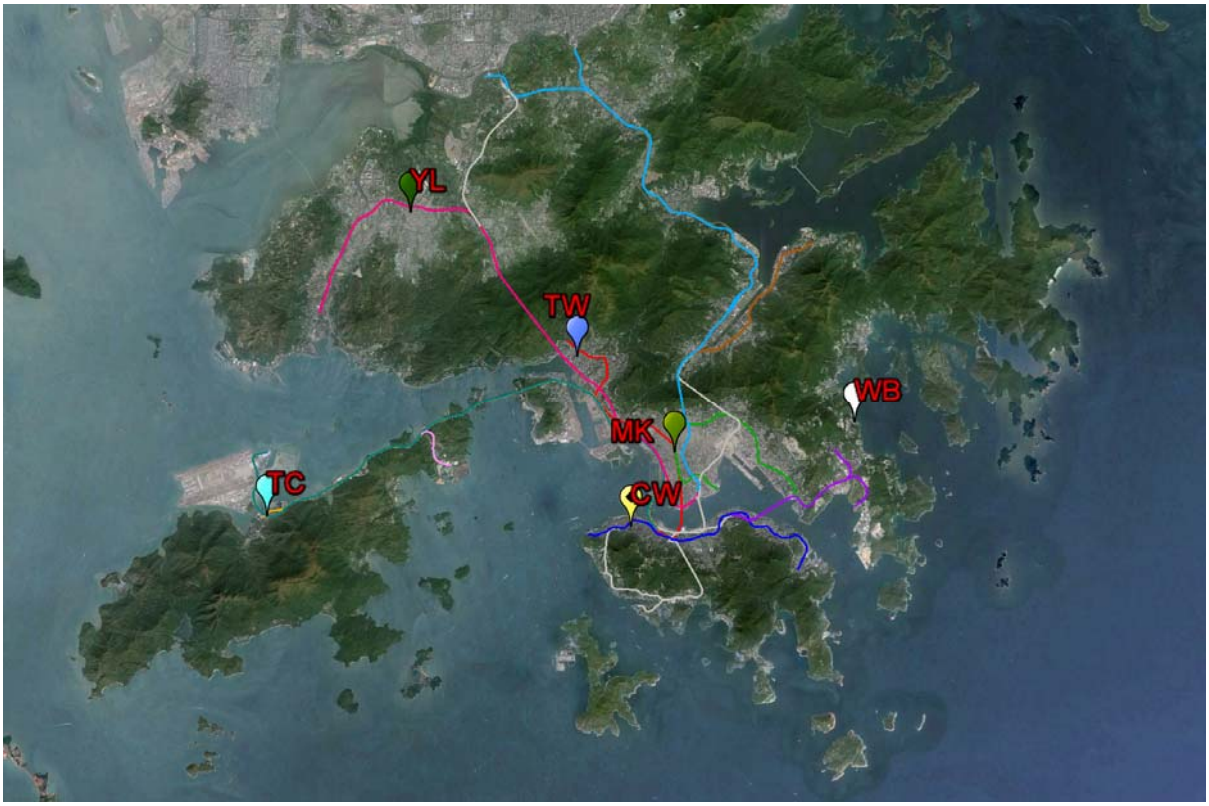

Figure S1 Data from six Hong Kong Air Quality Monitoring Sites (AQMS) are used in this study, including a roadside site Mong Kok (MK), four urban sites Central/Western (CW), Tsuen Wan (TW), Tung Chung (TC) and Yuen Long (YL), and a suburban site suburban Clear Water Bay (WB). The lines in different color represent the mass transit railway (MTR) in Hong Kong, which covers most urban areas (41% of population lives within 500 m of MTR station (Tang et al., 2004)).

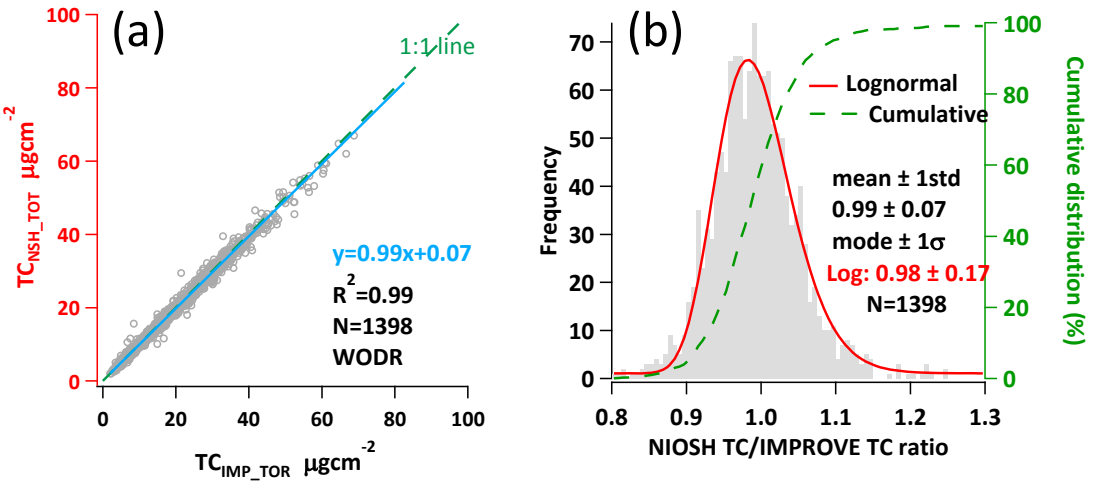

Figure S2 Comparison of total carbon quantification by IMPROVE TOR and NIOSH TOT protocols. (a) Scatter plot with weighted orthogonal distance regression (WODR). (b) Histogram of NIOSH TC/IMPROVE TC ratio.

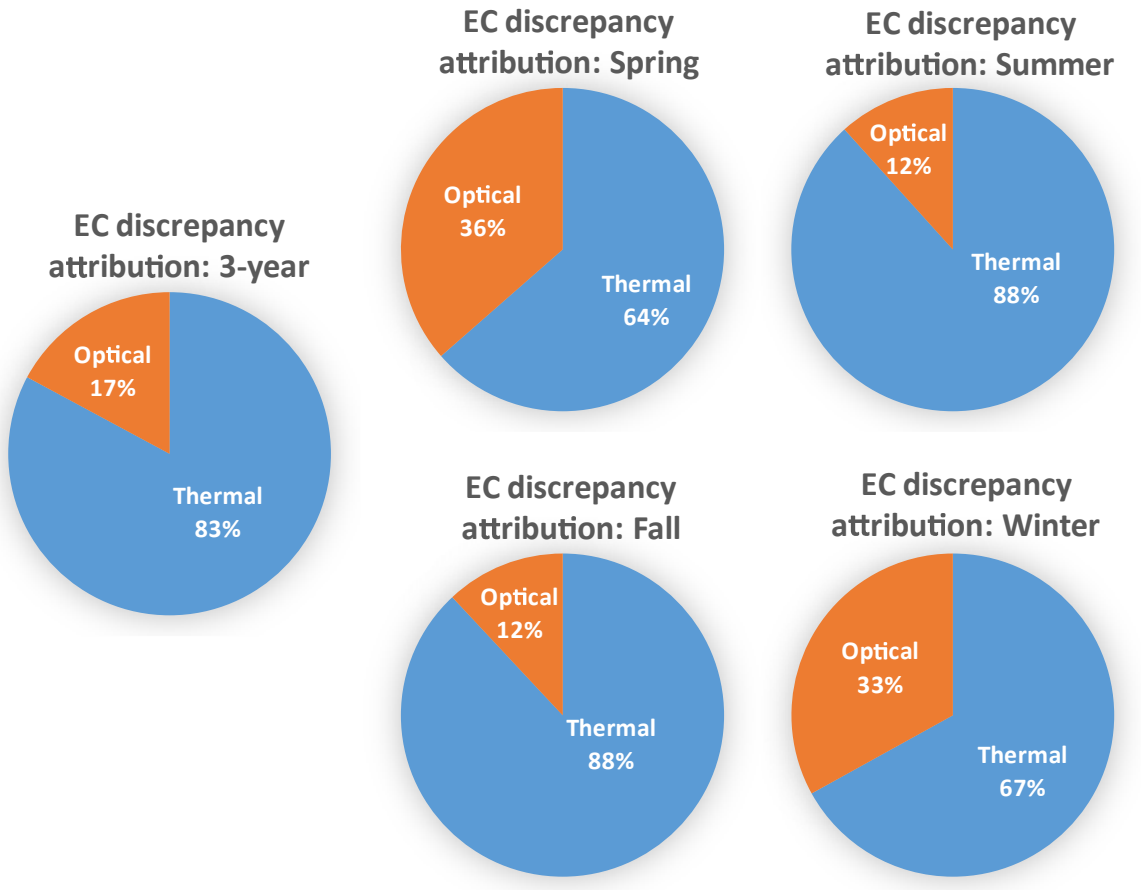

Figure S3 Seasonal variations of EC discrepancy attribution (optical method effect vs. thermal effect).

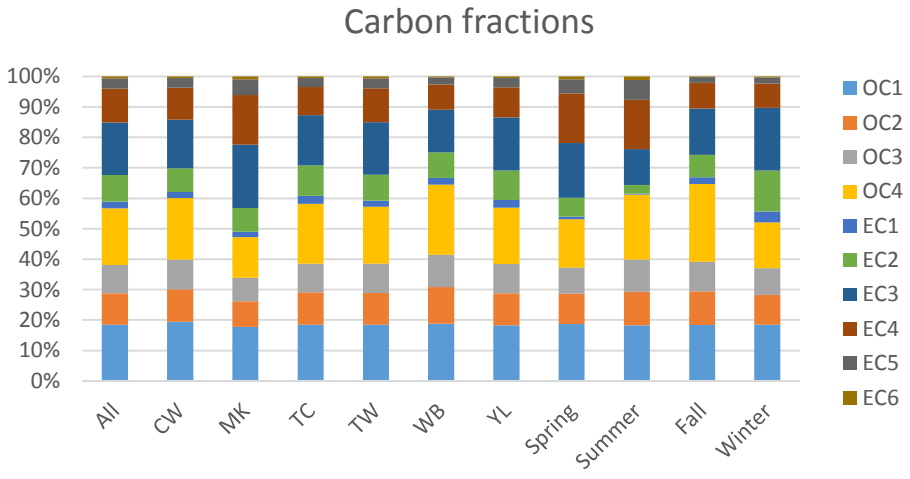

Figure S4 Inter-site and seasonal variations of NIOSH carbon fractions in HK samples (2011-2013).

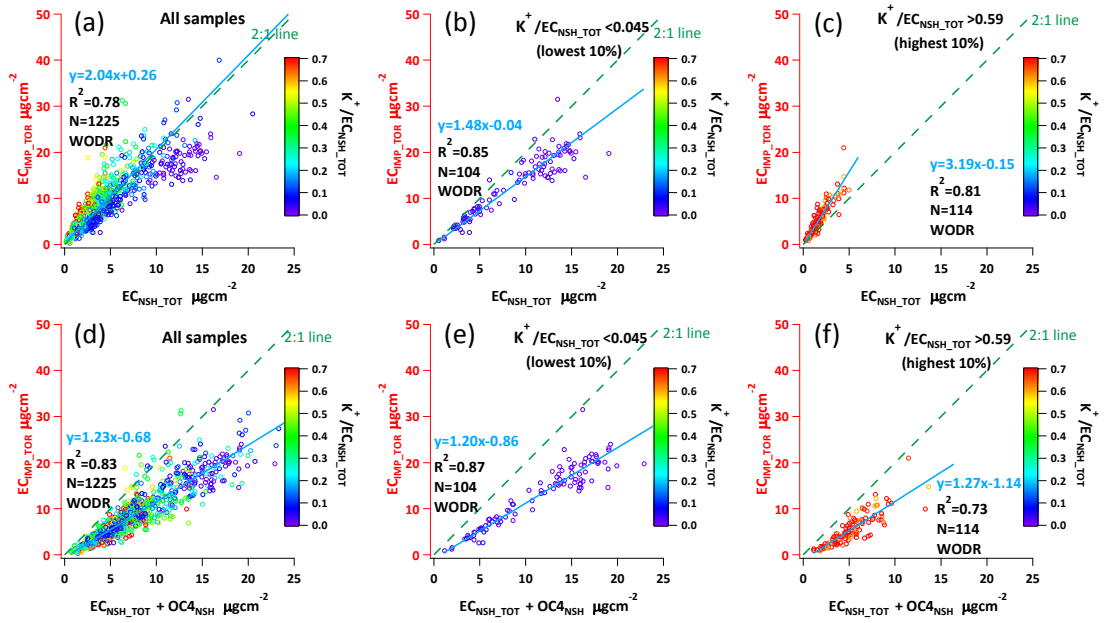

Figure S5 Scatter plots with linear regressions between IMPROVE TOR EC (EC_{IMP_TOR}) and NIOSH TOT EC (EC_{NSH_TOT}). The slopes represent the degree of discrepancy between the two protocols on EC determination. The color coding represents K^+/EC_{NSH} ratio, higher values are more likely associated with biomass influence. (a)~(c) EC_{IMP_TOR} in y axis and EC_{NSH_TOT} in x axis. (a) All samples. (b) Samples with lowest 10% K^+/EC_{NSH} ratio. (c) Samples with highest 10% K^+/EC_{NSH} ratio. (d)~(f) EC_{IMP_TOR} in y axis and EC_{NSH_TOT}+$OC4_{NSH}$ in x axis. (d) All samples. (e) Samples with lowest 10% K^+/EC_{NSH} ratio. (f) Samples with highest 10% K^+/EC_{NSH} ratio.

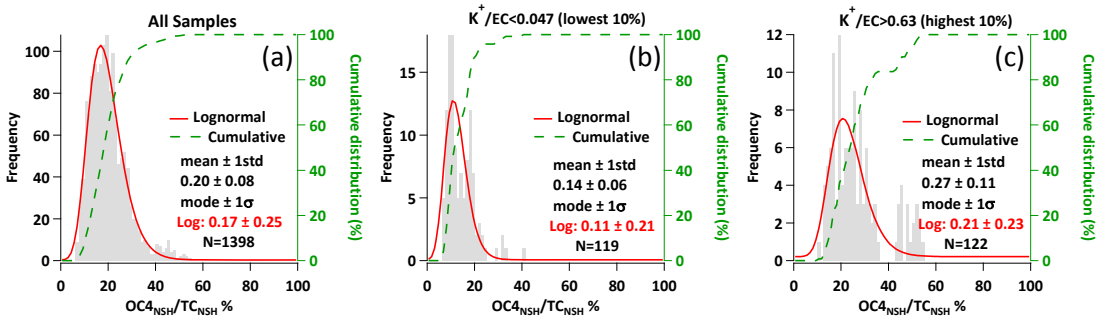

Figure S6 Frequency distributions of $OC4_{NSH}$ /TC ratio. (a) All samples. (b) Samples with lowest 10% K^+/EC_{NSH} ratio. (c) Samples with highest 10% K^+/EC_{NSH} ratio.

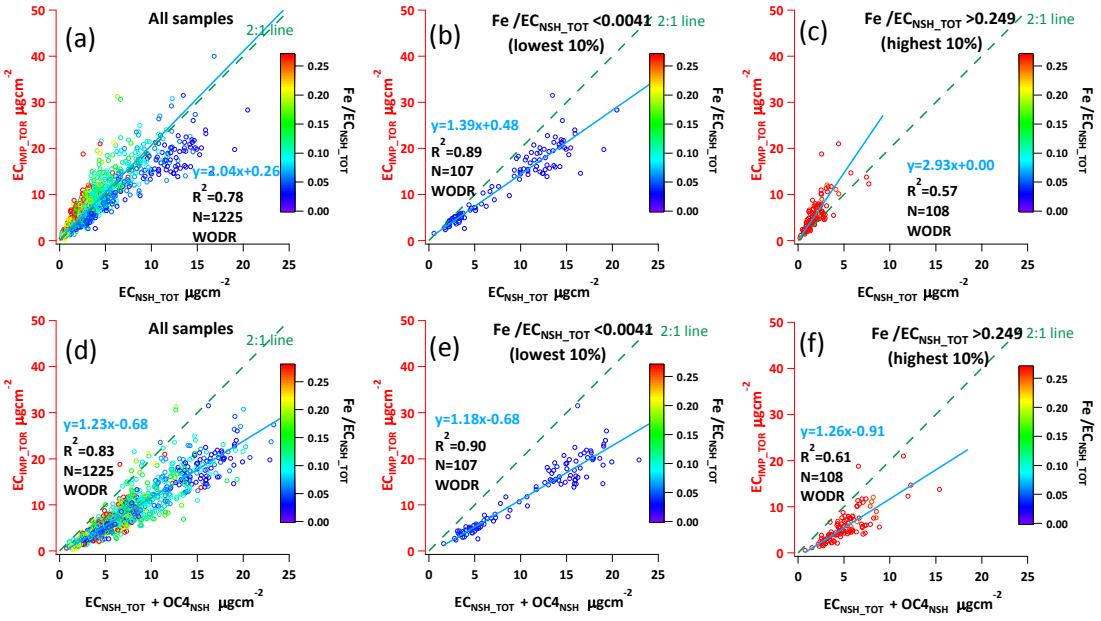

Figure S7 Scatter plots with linear regressions between IMPROVE TOR EC (EC_{IMP_TOR}) and NIOSH TOT EC (EC_{NSH_TOT}). The slopes represent the degree of discrepancy between the two protocols on EC determination. The color coding represents Fe/EC_{NSH} ratio. (a)~(c) EC_{IMP_TOR} in y axis and EC_{NSH_TOT} in x axis. (a) All samples. (b) Samples with lowest 10% Fe/EC_{NSH} ratio. (c) Samples with highest 10% Fe/EC_{NSH} ratio. (d)~(f) EC_{IMP_TOR} in y axis and EC_{NSH_TOT}+$OC4_{NSH}$ in x axis. (d) All samples. (e) Samples with lowest 10% Fe/EC_{NSH} ratio. (f) Samples with highest 10% Fe/EC_{NSH} ratio.

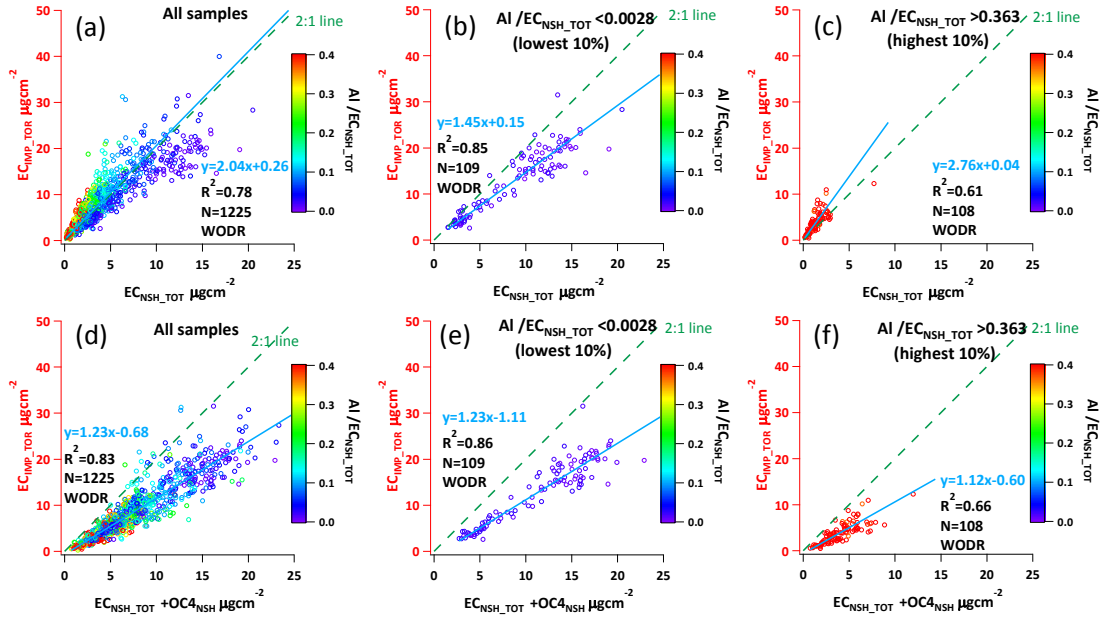

Figure S8 Scatter plots with linear regressions between IMPROVE TOR EC (EC_{IMP_TOR}) and NIOSH TOT EC (EC_{NSH_TOT}). The slopes represent the degree of discrepancy between the two protocols on EC determination. The color coding represents Al/EC_{NSH} ratio. (a)~(c) EC_{IMP_TOR} in y axis and EC_{NSH_TOT} in x axis. (a) All samples. (b) Samples with lowest 10% Al /EC_{NSH} ratio. (c) Samples with highest 10% Al /EC_{NSH} ratio. (d)~(f) EC_{IMP_TOR} in y axis and $EC_{NSH\_TOT}+OC4_{NSH}$ in x axis. (d) All samples. (e) Samples with lowest 10% Al /EC_{NSH} ratio. (f) Samples with highest 10% Al /EC_{NSH} ratio.

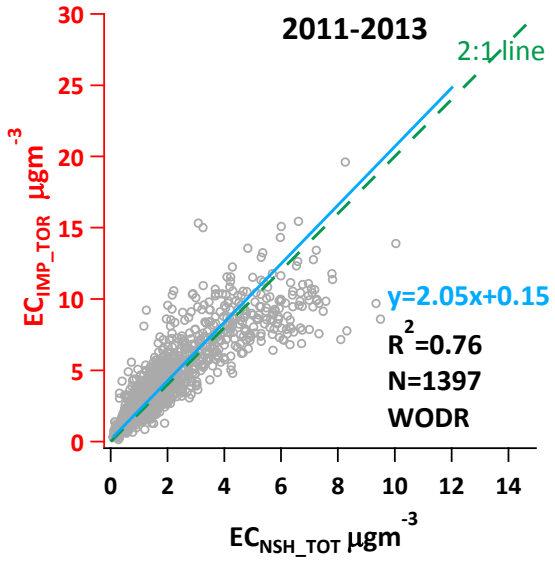

Figure S9 Linear regression between EC_{NSH_TOT} and EC_{IMP_TOR} for M1 reconstruction.

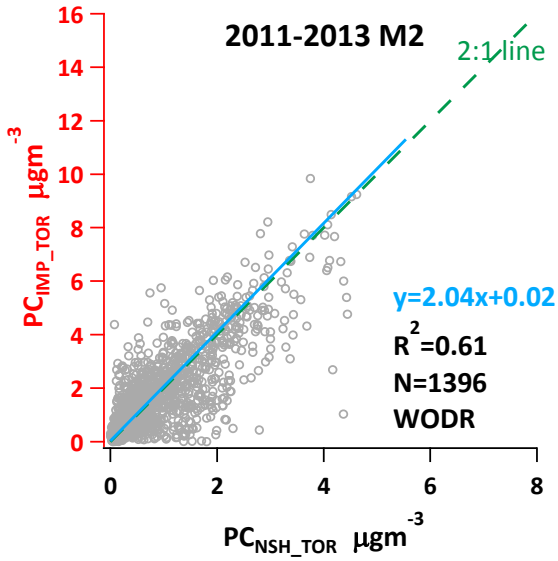

Figure S10 Linear relationship between PC_{NSH_TOR} and PC_{IMP_TOR} for M2 reconstruction.

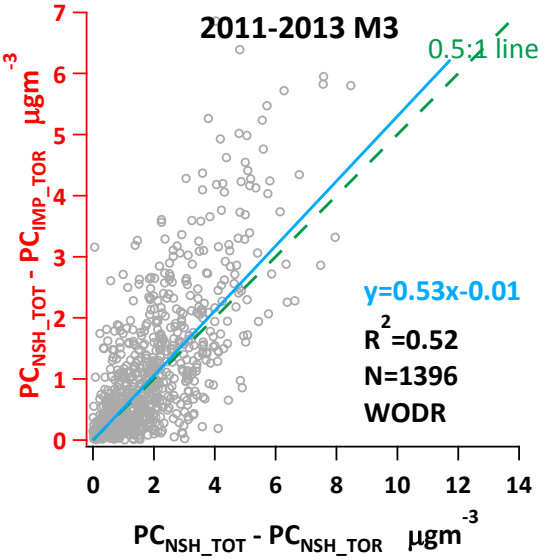

Figure S11 Linear relationship between PC_{NSH_TOT}-PC_{NSH_TOR} and PC_{NSH_TOT}-PC_{IMP_TOR} for M3 reconstruction.

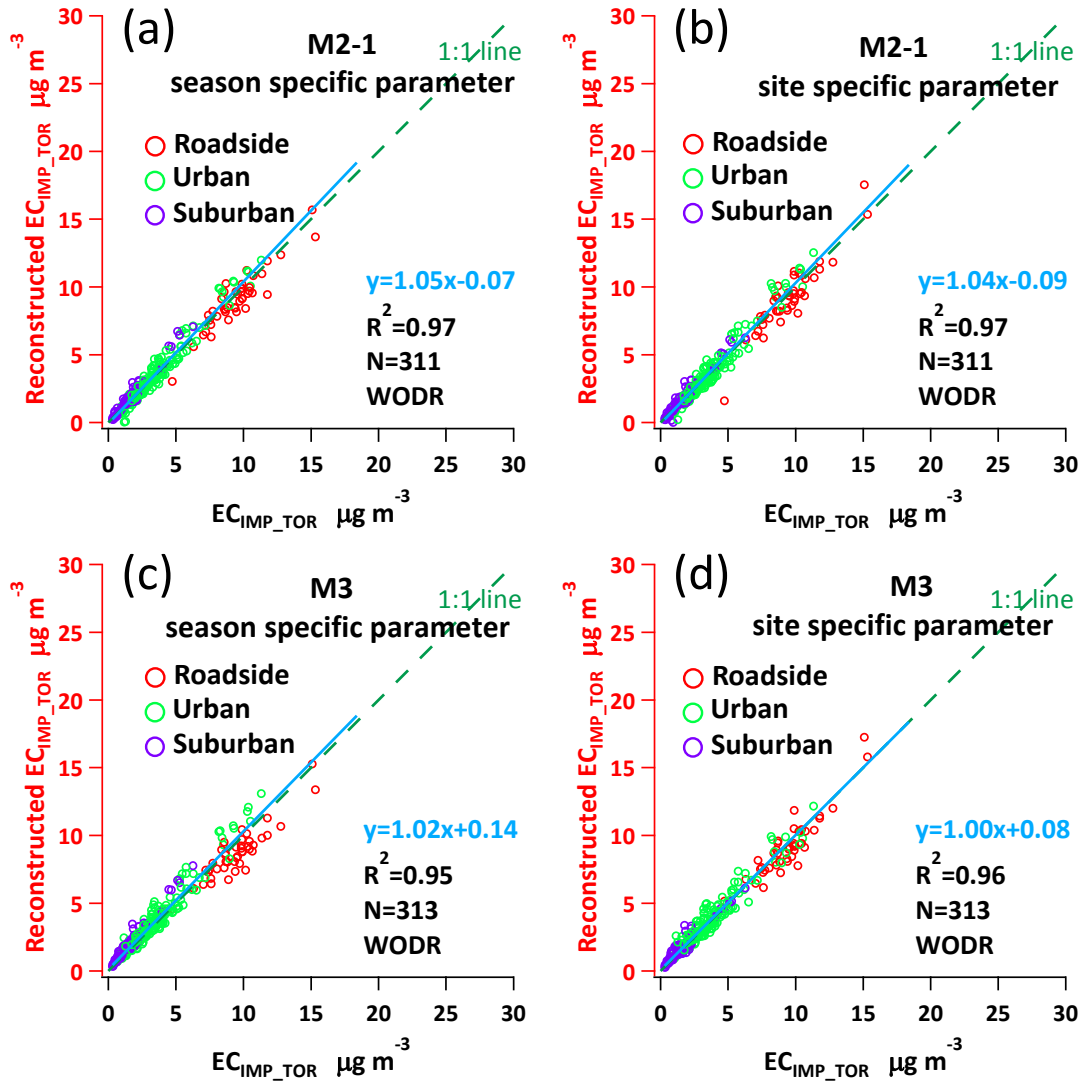

Figure S12 Comparison of reconstructed $\mathbf{EC_{IMP\_TOR}}$ and measurement EC_{IMP_TOR} in the year 2013. (a) Regression by season-specific parameters using M2-1. (b) Regression by site-specific parameters using M2-1. (c) Regression by season-specific parameters using M3. (d) Regression by site-specific parameters using M3.

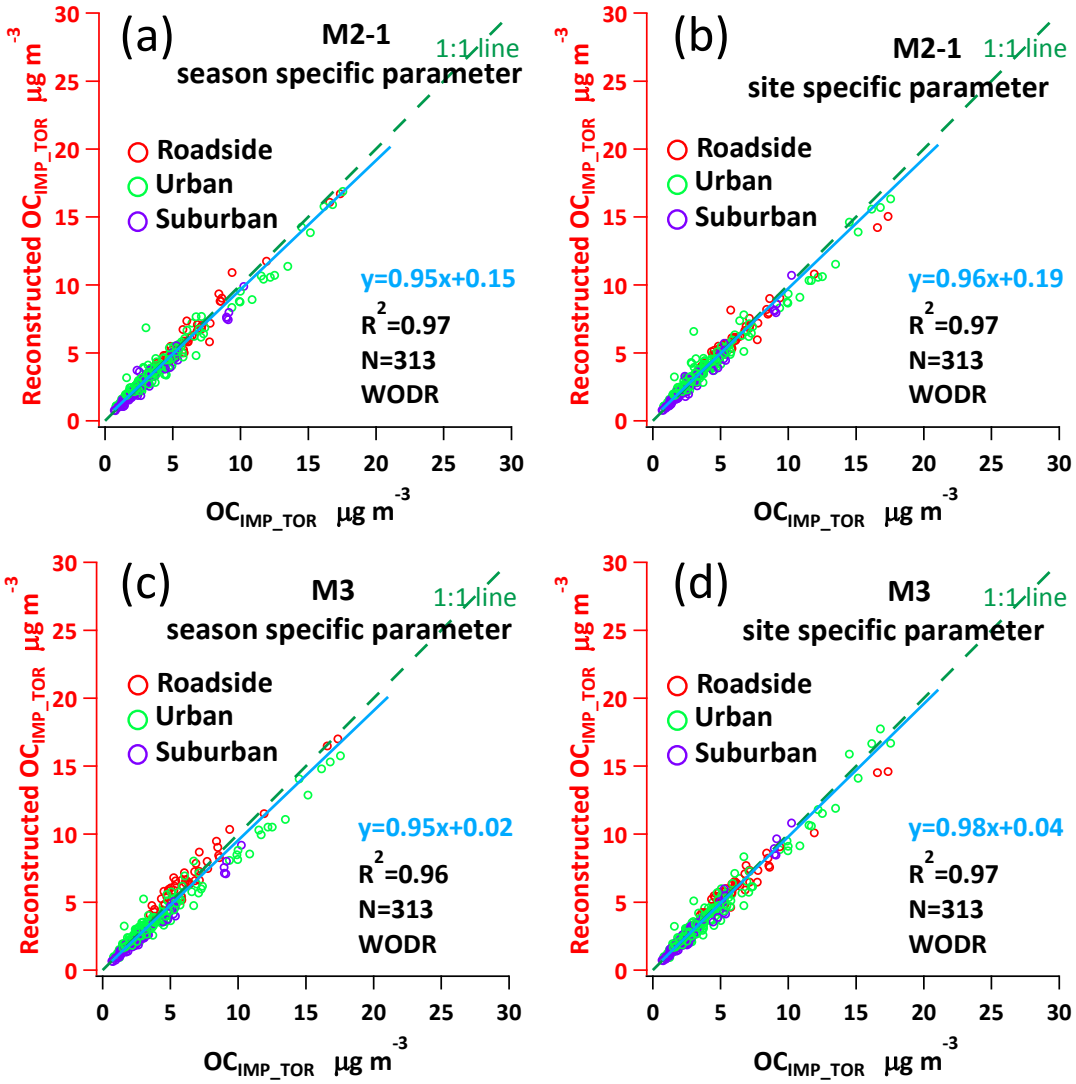

Figure S13 Comparison of reconstructed $\mathbf{OC_{IMP\_TOR}}$ and measurement OC_{IMP_TOR} in the year 2013. (a) Regression by season-specific parameters using M2-1. (b) Regression by site-specific parameters using M2-1. (c) Regression by season-specific parameters using M3. (d) Regression by site-specific parameters using M3.

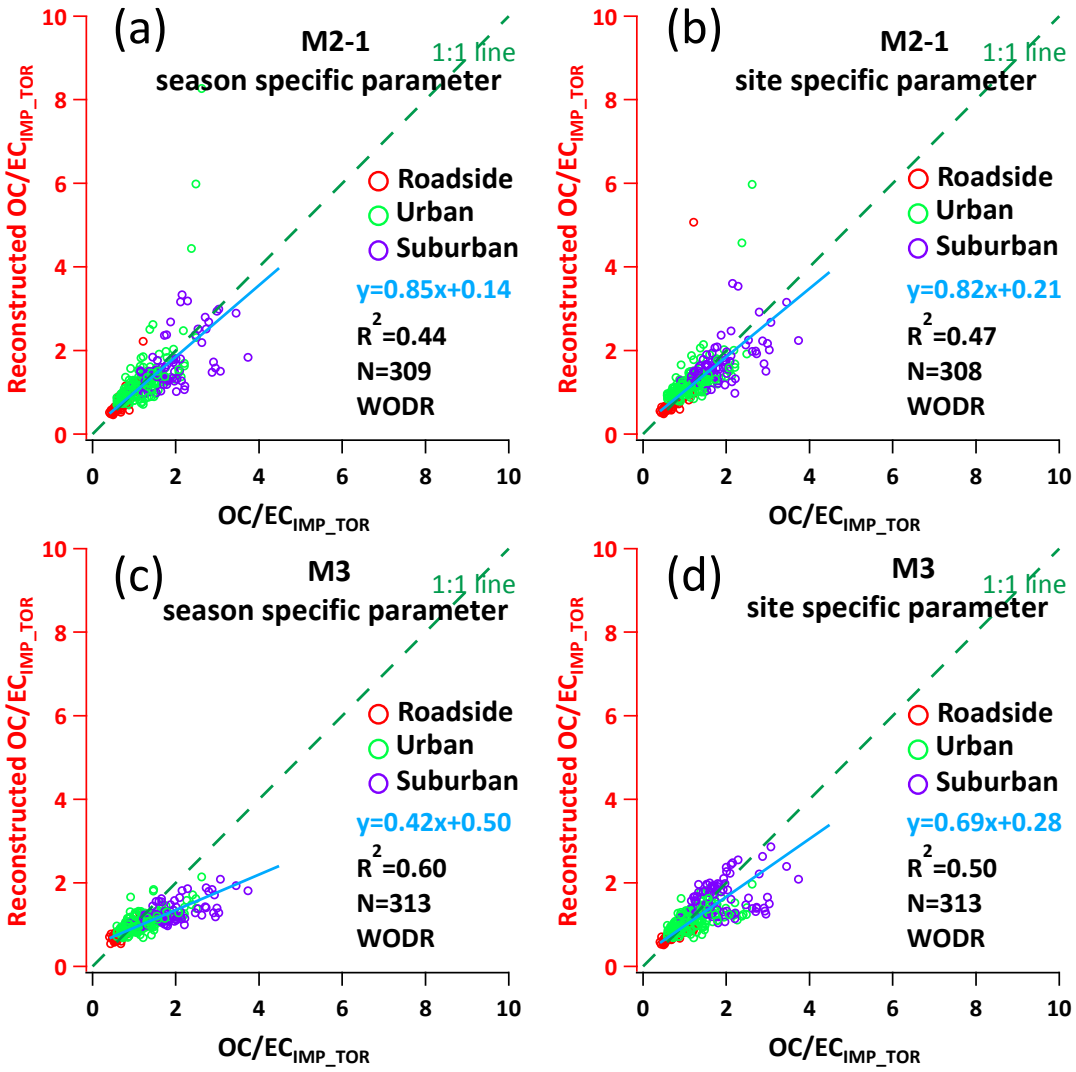

Figure S14 Comparison of reconstructed OC/EC_{IMP_TOR} and measurement OC/EC_{IMP_TOR} in the year 2013. (a) Regression by season-specific parameters using M2-1. (b) Regression by site-specific parameters using M2-1. (c) Regression by season-specific parameters using M3. (d) Regression by site-specific parameters using M3.

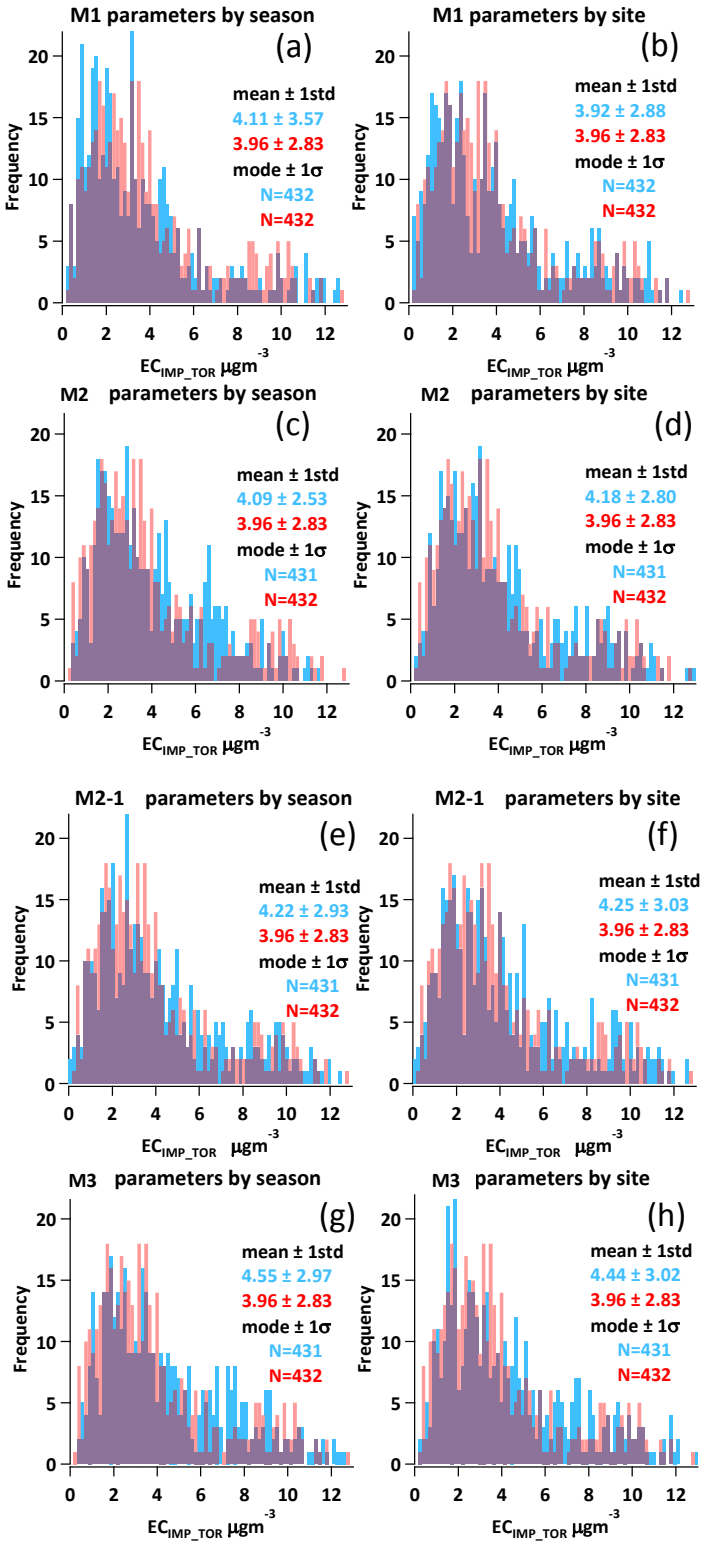

Figure S15 Frequency distributions of reconstructed EC (in blue) compared with measured EC (in red). The two distributions in each plot are overlaid, the darker color represents the overlapped areas of the two distribtuions. (a) Season-specific parameters using M1. (b) Site-specific parameters using M1. (c) Season-specific parameters using M2. (d) Site-specific parameters using M2. (e) Season-specific parameters using M2-1. (f) Site-specific parameters using M2-1. (g) Season-specific parameters using M3. (h) Site-specific parameters using M3.

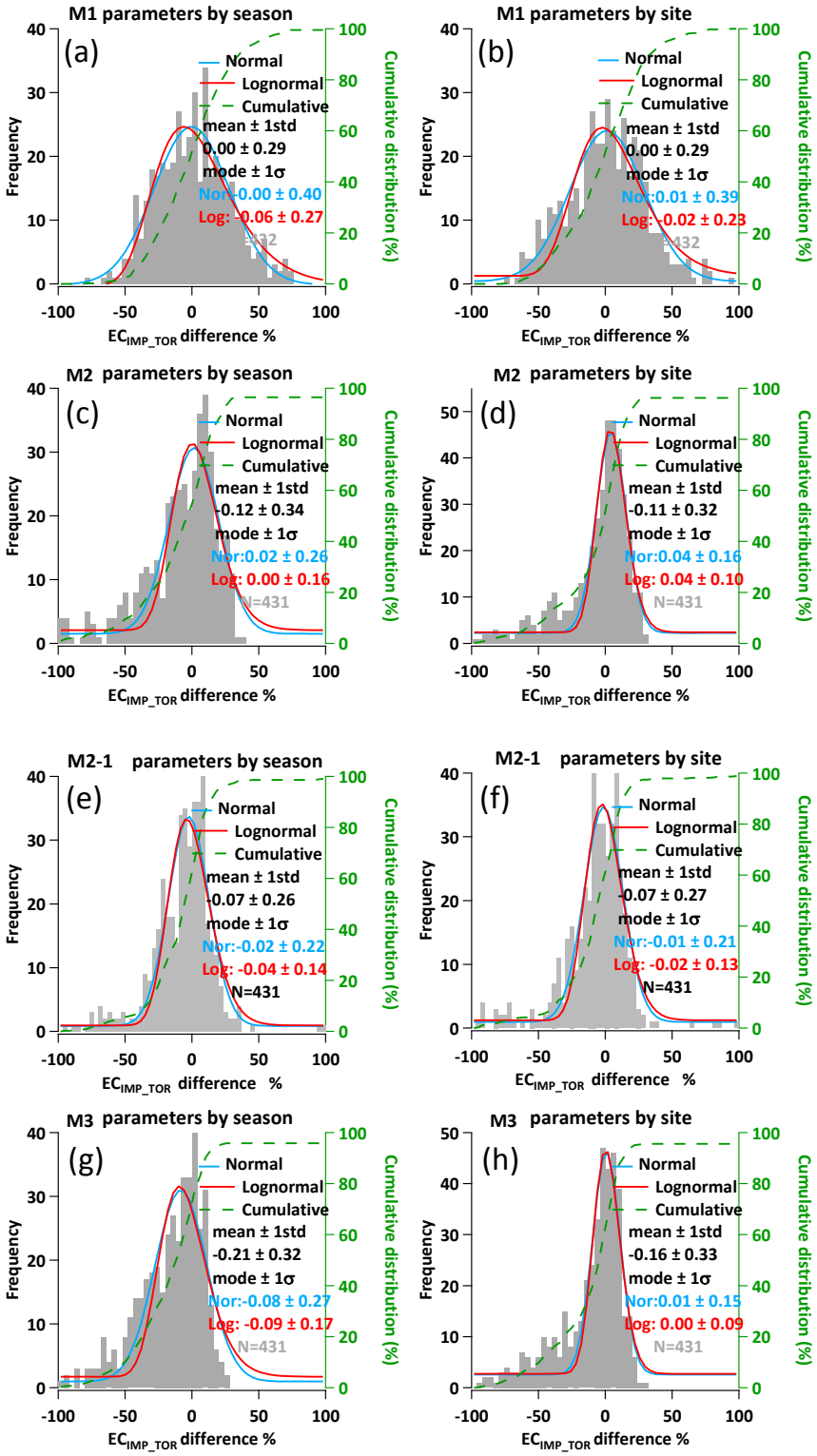

Figure S16 Frequency distributions of difference between reconstructed EC and measured EC. (a) Season-specific parameters using M1. (b) Site-specific parameters using M1. (c) Season-specific parameters using M2. (d) Site-specific parameters using M2. (e) Season-specific parameters using M2-1. (f) Site-specific parameters using M2-1. (g) Season-specific parameters using M3. (h) Site-specific parameters using M3.

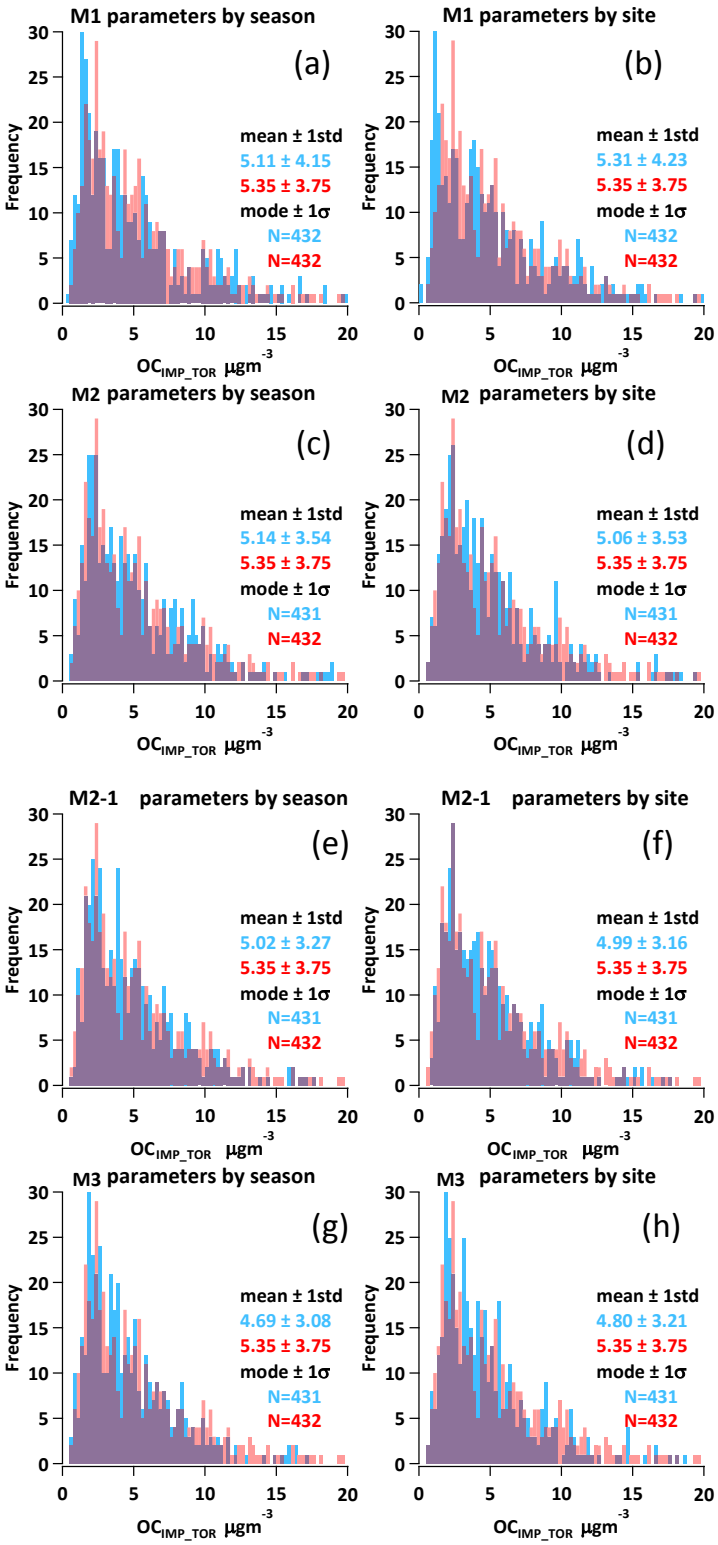

Figure S17 Frequency distributions of reconstructed OC (in blue) compared with measured EC (in red). The two distributions in each plot are overlaid, the darker color represents the overlapped areas of the two distribtuions. (a) Season-specific parameters using M1. (b) Site-specific parameters using M1. (c) Season-specific parameters using M2. (d) Site-specific parameters using M2. (e) Season-specific parameters using M2-1. (f) Site-specific parameters using M2-1. (g) Season-specific parameters using M3. (h) Site-specific parameters using M3.

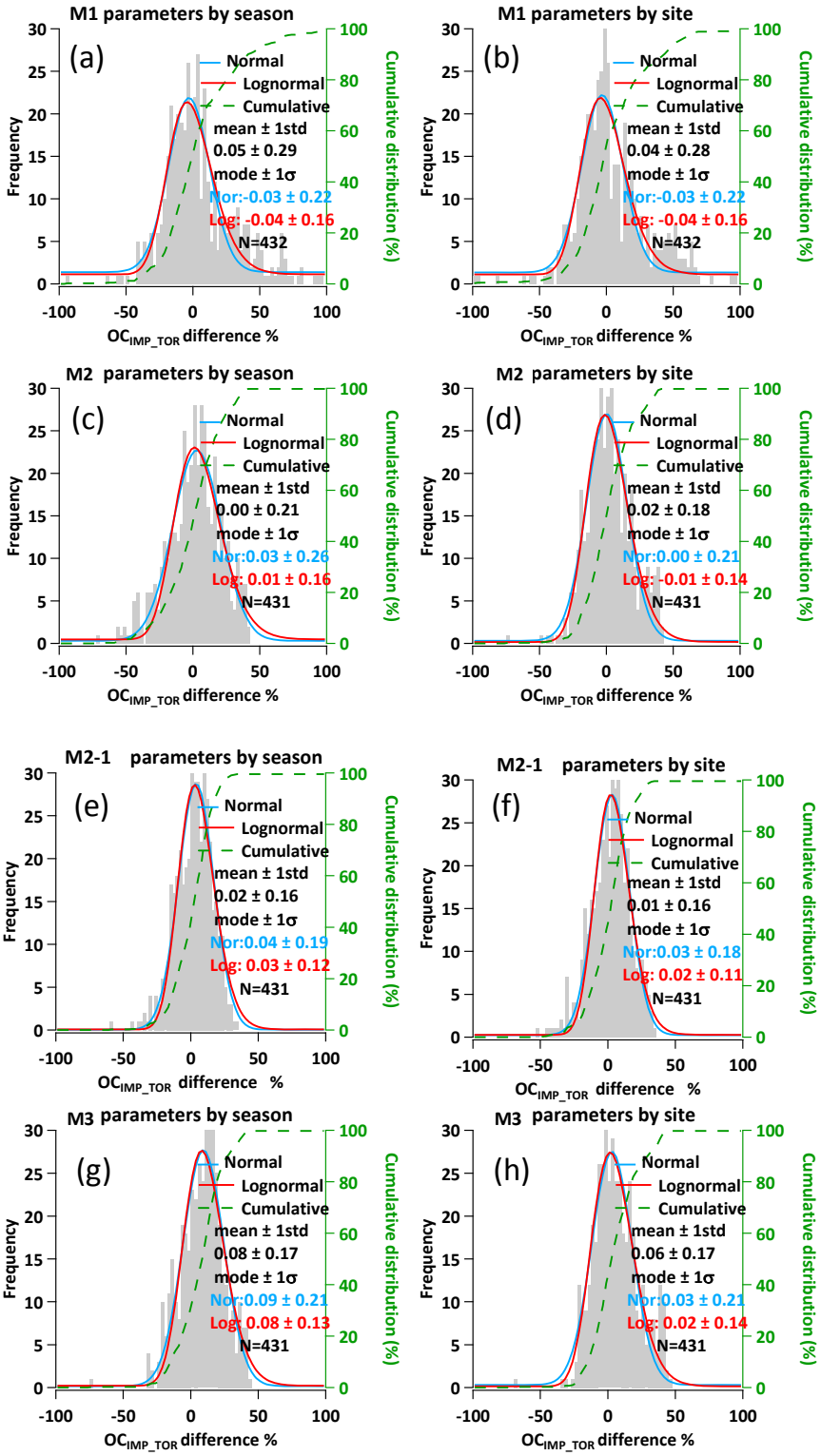

Figure S18 Frequency distributions of difference between reconstructed OC and measured OC. (a) Season-specific parameters using M1. (b) Site-specific parameters using M1. (c) Season-specific parameters using M2. (d) Site-specific parameters using M2. (e) Season-specific parameters using M2-1. (f) Site-specific parameters using M2-1. (g) Season-specific parameters using M3. (h) Site-specific parameters using M3.

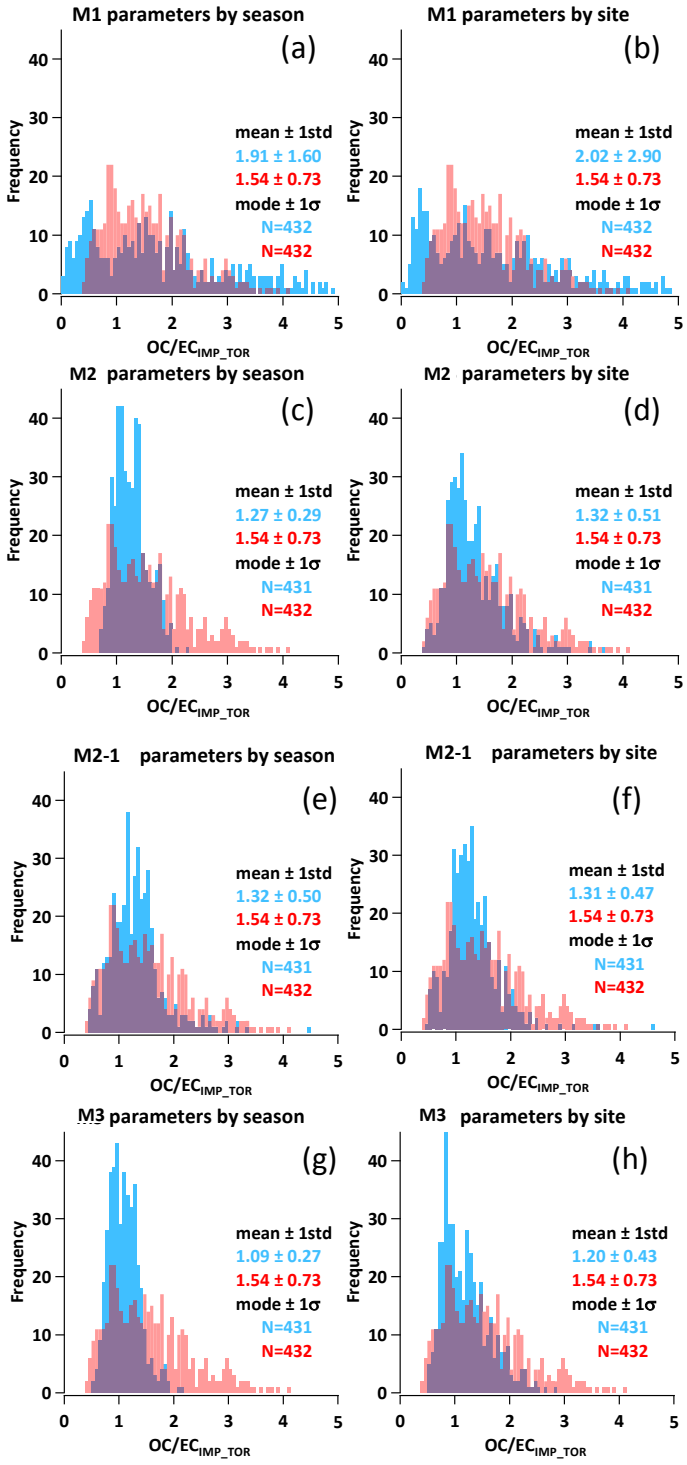

Figure S19 Frequency distributions of reconstructed OC/EC ratio (in blue) compared with measured OC/EC ratio (in red). The two distributions in each plot are overlaid, the darker color represents the overlapped areas of the two distribtuions. (a) Season-specific parameters using M1. (b) Site-specific parameters using M1. (c) Season-specific parameters using M2. (d) Site-specific parameters using M2. (e) Season-specific parameters using M2-1. (f) Site-specific parameters using M2-1. (g) Season-specific parameters using M3. (h) Site-specific parameters using M3.

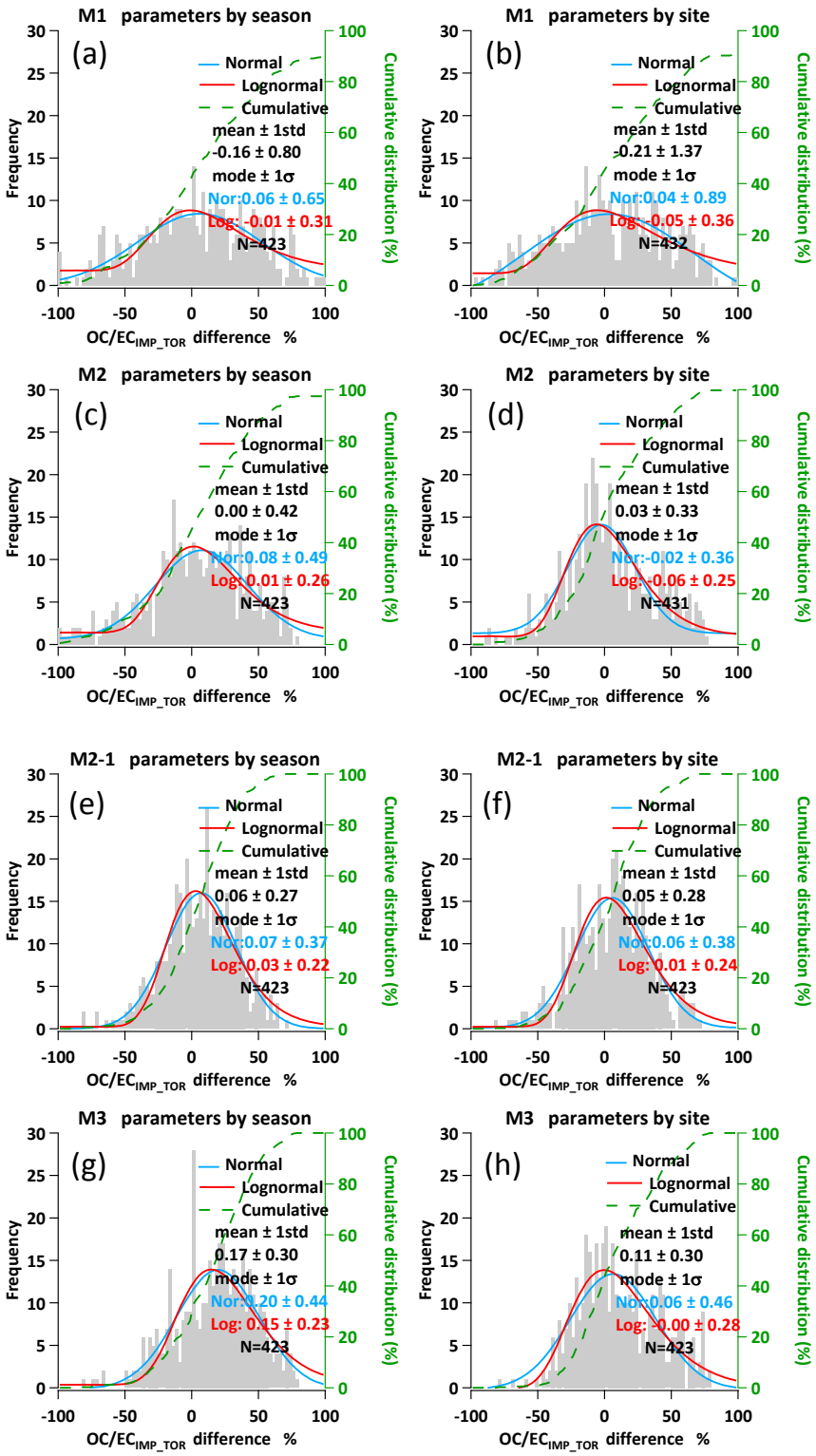

Figure S20 Frequency distributions of difference between reconstructed OC/EC and measured OC/EC. (a) Season-specific parameters using M1. (b) Site-specific parameters using M1. (c) Season-specific parameters using M2. (d) Site-specific parameters using M2. (e) Season-specific parameters using M2-1. (f) Site-specific parameters using M2-1. (g) Season-specific parameters using M3. (h) Site-specific parameters using M3.

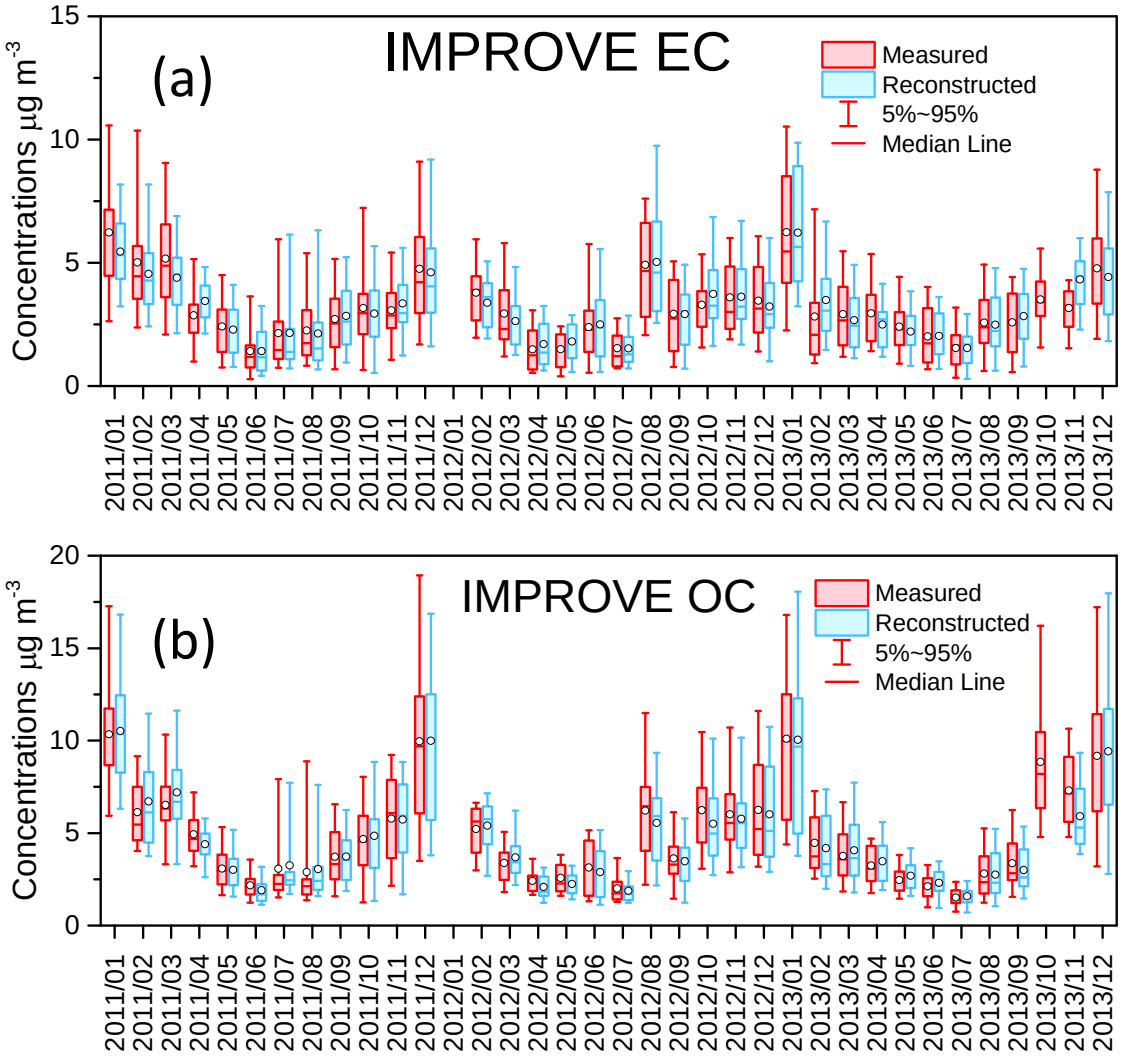

Figure S21 Monthly time series of measured and reconstructed EC and OC at 5 sites in HK (four urban sites Central/Western (CW), Tsuen Wan (TW), Tung Chung (TC) and Yuen Long (YL), and a suburban site suburban Clear Water Bay (WB)). The reconstruction uses M2 site-specific parameters obtained from 2011-2012 data as shown in Table 2. Sample size of Jan 2012 is too small and not included in the plot. Samples of Oct 2013 analyzed by NIOSH protocol did not pass QA/QC check, the so corresponding reconstructed results are not included in the plot.

.

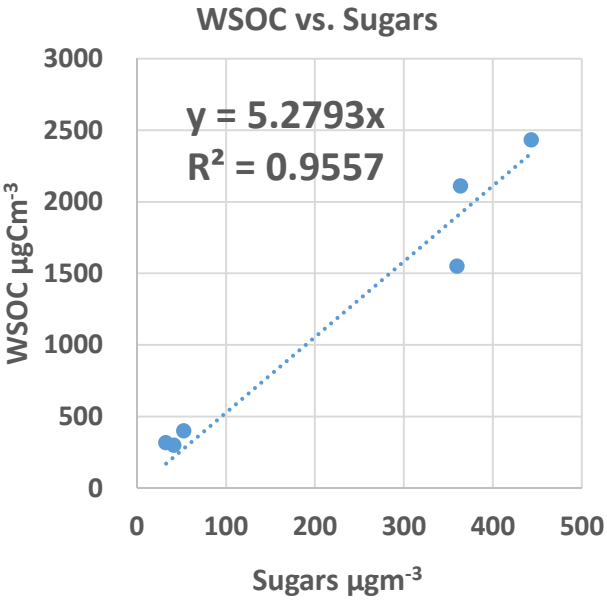

Figure S22 Primary ratio of WSOC/Sugars from an emission study in PRD region (Lin et al., 2010).

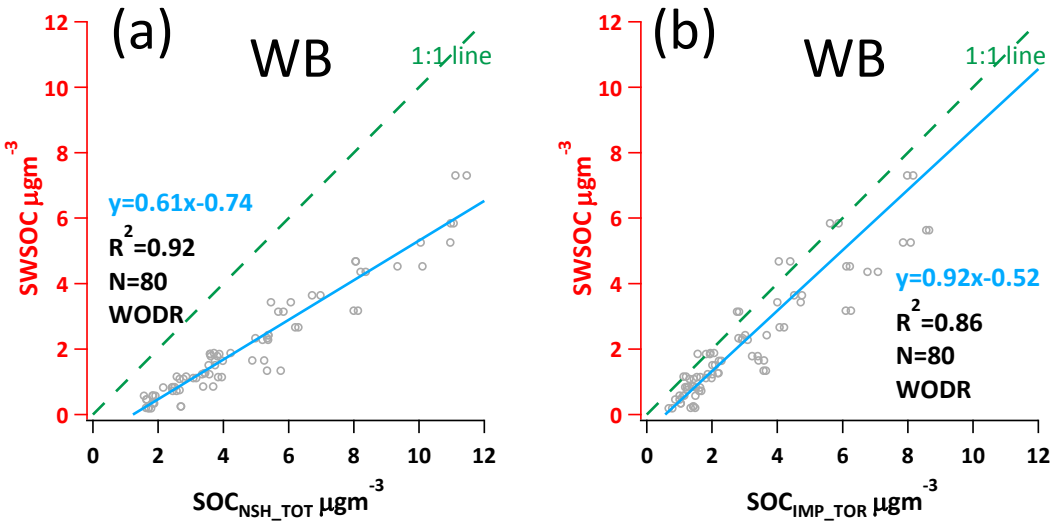

Figure S23 Linear regression between SWSOC and SOC at WB site. (a) SOC by NIOSH TOT (b) SOC by IMPROVE TOR.

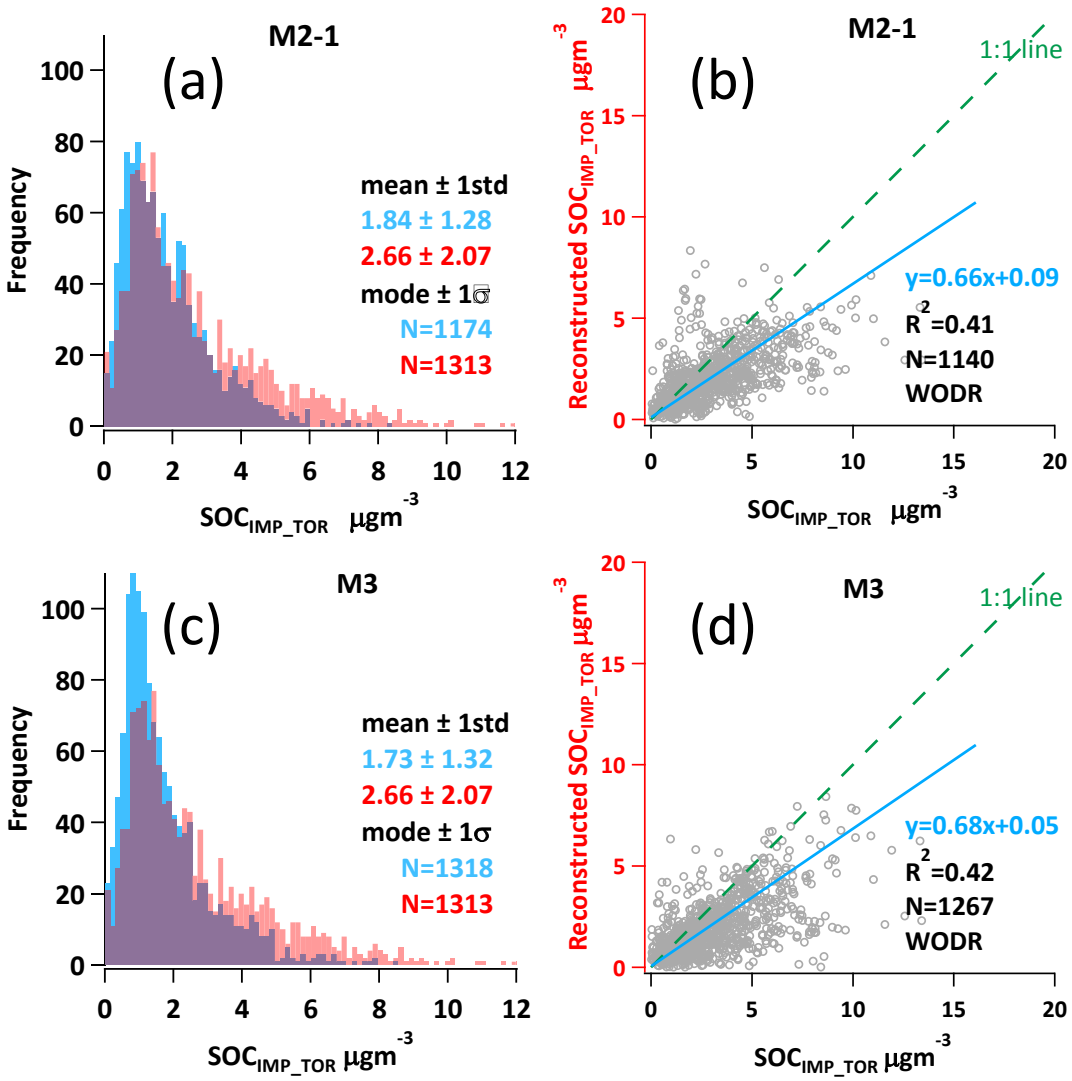

Figure S24 Histogram comparison of original SOC_{IMP_TOR} (in red) with reconstructed SOC_{IMP_TOR} (in blue): (a) by M2-1. (c) by M3. The two distributions in each plot are overlaid, the darker color represents the overlapped areas of the two distribtuions. Scatter plot comparison of original SOC_{IMP_TOR} (in x axis) with reconstructed SOC_{IMP_TOR} (in y axis): (b) by M2-1, (d) by M3.